https://doi.org/10.5194/egusphere-2026-6224
Preprint. Discussion started: 4 November 2026
© Author(s) 2026. CC BY 4.0 License.

Quality Consistency Assessment among MODIS, MERSI, and VIIRS Cloud Mask Products using China's Space-borne Lidar ACDL

Sijie Chen[1,2], Bo Li[1,2], Xi Wang[1,2], Zhaojun Zheng[1,2], Lin Chen[1,2], and Jian Liu[1,2*]

[1]The Key Laboratory of Radiometric Calibration and Validation for Environmental Satellites, National Satellite Meteorological Center (National Center for Space Weather), China Meteorological Administration, Beijing, 100081, China
[2]The Innovation Center for FengYun Meteorological Satellite, Beijing, 100081, China

Correspondence to: Jian Liu (liujian@cma.cn)

Abstract. Cloud masking is the fundamental step in accurately retrieving cloud and many other properties from satellite-based imagers. Intercomparisons among imagers are frequently conducted to assess the agreement of cloud masks at both global and granule scales, ensuring accuracy while also enabling the merging of multi-satellite products for use in NWP models and climate datasets. However, common challenges arise in scenarios with reduced spectral contrast between clouds and backgrounds, leading to generally degraded performance at polar regions and making validation through intercomparison less reliable. Building on previous synergistic observations between CALIOP and MODIS in the A-Train constellation, this study employed China's Aerosol and Carbon Detection Lidar (ACDL) as a new benchmark to evaluate cloud masks from 3 passive sensors across different operational stages. Analyzing approximately 3 million collocated samples in February and August 2024, the overall hit rates for confident cloudy/clear pixels from Aqua/MODIS, FY-3D/MERSI-II, and NOAA-21/VIIRS reached 82.9%, 79.3%, and 86.4%, respectively. Detailed examinations of monthly, day/night, and latitudinal subsets revealed variation in each sensor's performance across scenerios and identified the reasons behind the discrepancies. The study highlighted the importance of active-passive validation, which confirms consistency among passive imagers while also identifying algorithmic weaknesses that need improvement for future missions.

1 Introduction

In recent decades, advances in space-borne imaging have enabled us to observe and quantify the global distribution of clouds, and cloud masking, the process of identifying cloudy pixels in satellite imagery, has become increasingly important for both the accurate retrieval of cloud properties (Wu et al. 2018) and for preventing cloud-induced biases (Sedano et al. 2011). Since most satellite imagers rely on using multispectral radiance measurements to distinguish cloudy from clear-sky pixels, they face common challenges for optically thin clouds and over highly reflective surfaces, such as snow- and ice-covered polar regions. (Ackerman et al. 1998; Meyer et al. 2020). These shared limitations may compromise the reliability of cloud mask validation based on intercomparisons among different satellite imagers. Therefore, independent validation using space-borne lidar, which employs a fundamentally different principle from that of passive imagers, is essential to accurately assess and improve the quality of cloud mask products, particularly in polar regions.

https://doi.org/10.5194/egusphere-2026-6224
Preprint. Discussion started: 4 November 2026
© Author(s) 2026. CC BY 4.0 License.

In 2006, NASA and CNES jointly launched the Cloud-Aerosol Lidar with Orthogonal Polarization (CALIOP) on board the Cloud-Aerosol Lidar and Infrared Pathfinder Satellite Observation (CALIPSO) satellite (Winker et al. 2009). As a space-borne lidar, CALIOP actively emits laser pulses to measure atmospheric structures, offering the advantages of high vertical resolution (30 to 180 m from near-surface to stratosphere) and independence from illumination conditions. Validation reports that CALIOP retrievals agree with ground-based lidars in most cases, with cloud height uncertainties less than 0.51 km (Thorsen, Fu, and Comstock 2011), but have difficulty determining the underlying thick clouds beneath thin cirrus due to signal attenuation (Kim et al. 2011).

CALIOP establishes a widely accepted reference for cloud mask products, especially for other sensors in the A-Train satellite constellation. With formation flying, CALIOP has conducted synchronized observations with the Moderate Resolution Imaging Spectroradiometer (MODIS) onboard the Aqua satellite(Ackerman et al. 2008) on a long-term basis. Holz et al. (2008) found that the global agreement between CALIOP and MODIS exceeded 80% for clear and cloudy conditions based on two months of observation, while Kotarba et al. (2020) further calibrated CALIOP profiles to each of four MODIS mask categories. The results of comparisons have made important contributions to refining the MODIS cloud mask algorithm from C5 to C6 (Baum et al. 2012). In 2011, 2017, and 2022, NASA developed and launched MODIS' successor payloads, the Visible Infrared Imaging Radiometer Suite (VIIRS), the latest of which is NOAA-21 (Xiong et al. 2023). VIIRS features radiation in 22 bands instead of 36 for MODIS, and its orbits are no longer part of the A-Train constellation. As a result, CALIOP profiles have fewer high-quality collocated pixels with VIIRS, but the agreement remains promising (Kopp et al. 2014; Frey et al. 2020).

After CALIOP retired in Aug. 2023, new spaceborne lidars are needed to continue validating cloud mask products. In 2022, China launched the Daqi-1 (DQ-1) satellite, carrying the Aerosol and Carbon Detection Lidar (ACDL). ACDL employs a high-spectral-resolution lidar (HSRL) technique, enabling independent retrieval of the lidar ratio (Ke et al. 2022), and therefore exhibits higher inversion accuracy than traditional Mie-scattering lidars. Dai et al. (2024) detailed ACDL's aerosol and cloud data processing, highlighting its polarization sensitivity for distinguishing cloud phases. Liu et al. (2024) validated ACDL's initial observations against ground-based lidars, with total attenuated backscatter coefficients agreeing to within $10.5 \pm 25.4\%$ and cloud heights matching well. ACDL has also been applied in comparisons and synergistic observations with the Medium Resolution Spectral Imagers-II (MERSI-II) onboard FengYun (FY)-3D, China's polar-orbiting meteorological satellites (Chen et al. 2025).

In this paper, we employed data from Aqua/MODIS, FY-3D/MERSI-II, and NOAA-21/VIIRS in Feb. and Aug. 2024 and compared their cloud-mask products with ACDL profiles. Results from 3 passive payloads at different operational stages gave an evaluation of cloud mask accuracy across diverse conditions, while also enabling assessments of consistency between ACDL-based and previous CALIOP-based validations.

The following sections are organized as follows: Section 2 briefly overviews the payload configurations of active and passive sensors used in the study and their cloud products; Section 3 demonstrates the results of comparisons, including global distributions of clouds from different sensors and associated analyses; Section 4 compares the results with previous studies,

https://doi.org/10.5194/egusphere-2026-6224
Preprint. Discussion started: 4 November 2026
© Author(s) 2026. CC BY 4.0 License.

analyzes influential factors, and discusses limitations; Section 5 provides conclusions, emphasizing implications for future satellite remote sensing advancements.

2 Data and method

This study investigates global cloud distribution using three passive satellite imagers (Aqua/MODIS, FY-3D/MERSI-II, and NOAA-21/VIIRS) and evaluates their performance against ACDL lidar cloud profiles. The analysis focuses on spatially and temporally collocated observations within 82°S–82°N, constrained by the lidar footprint. Two representative months (Feb. and Aug. 2024) were selected to capture seasonal contrasts.

2.1 Instrument and platforms

Three passive sensors in afternoon orbits were selected to ensure optimal synergy with ACDL observations. Aqua/MODIS (launched in 2002), FY-3D/MERSI-II (2017), and NOAA-21/VIIRS (2022) provide long-term continuity and inter-comparable measurements due to their similar spectral configurations and product design. Additional details of the passive instrument design are provided in the Appendix A.

ACDL, launched in 2022, is a spaceborne three-wavelength lidar system. In this study, only the HSRL profiles were used to derive vertical cloud profiles, a mechanism that allowed separation of aerosol contribution from molecular backscatter, thereby removing the lidar ratio assumption in the Mie-scattering lidar derivation (Liu et al. 2013). Initial validation indicated an accuracy better than 20% for a strong signal backscatter profile with 24 m vertical resolution(Chen et al. 2023).

Table 1: Orbit and instrument design of Aqua/MODIS, FY-3D/MERSI-II, NOAA-21/VIIRS, and DQ-1/ACDL

Satellite Instrument	Aqua MODIS	FY-3D MERSI-II	NOAA-21 VIIRS	DQ-1 ACDL
Orbit	Sun-synchronous	Sun-synchronous	Sun-synchronous	Sun-synchronous
Altitude	705 km	836 km	833 km	705 km
Inclination	98.2°	98.75°	98.7°	98.2°
Period	~99 min	~101.5 min	~101.5 min	~99 min
Crossing time	13:30 (Ascending)	13:45-14:00 (Ascending)	13:30 (Ascending)	13:30 (Ascending)
Instrument	Scanning radiometer	Scanning radiometer	Scanning radiometer	HSRL
Swath	2330 km	2900 km	3040 km	-
# Bands	36	25	22	532/1064 nm
Temporal resolution	5 min	5 min	6 min	-
Spatial resolution	250/500/1000 m	250/1000 m	375/750 m	Track: 333 m Vertical: 24 m

https://doi.org/10.5194/egusphere-2026-6224
Preprint. Discussion started: 4 November 2026
© Author(s) 2026. CC BY 4.0 License.

2.2 Products and retrieval algorithms

For passive sensors, official L2 cloud mask products and L3 monthly cloud fraction datasets were used. These products are based on multispectral threshold and consistency tests exploiting spectral contrasts between clouds and surface backgrounds (e.g., visible reflectance and thermal infrared brightness temperature differences). Despite differences in spectral band configurations, MODIS, VIIRS, and MERSI-II adopt similar cloud-detection principles, ensuring general consistency in cloud-mask products(See Table A1). VIIRS uses a continuity cloud mask (MVCM) to maintain consistency with MODIS, while MERSI-II applies comparable threshold-based methods.

ACDL cloud profiles were derived from attenuated backscatter signals using established layer detection and classification approaches. The processing includes signal averaging, molecular calibration using ERA5 atmospheric profiles, and cloud–aerosol discrimination based on backscatter characteristics, described in Dai et al. (2024) and Ke et al. (2022).

Since ACDL measurements have not yet been released as official products, the procedures were briefly summarized here. The core parameter is the backscatter coefficient ratio (R_a), which is the relative magnitude between particle and molecular signals. Theoretically, atmospheric features are identified when $R_a > 1$, with values exceeding 5 typically classified as clouds. It is calculated as follows:

$$\beta_a(z) = \beta_m(z)\frac{[1+\delta(z)][f_m(z)-f_a]R(z)}{(1+\delta_m)[1-f_aR(z)]} - \beta_m(z), \quad (1)$$

where $\beta_a(z)$ is the particulate backscattering coefficient at height z; $\beta_m(z)$ is the molecular backscattering coefficient; $\delta(z)$is the total depolarization ratio; $f_m(z)$ and f_a are the transmittance of the iodine absorption filter for molecular and aerosol scattering, respectively; $R(z)$ is the backscattering ratio between the 532 nm parallel channel and the HSRL channel signals; and δ_m is molecular depolarization ratio constant.

The $\delta(z)$ was calculated as

$$\delta(z) = \frac{\beta_m^{\perp}(z)+\beta_a^{\perp}(z)}{\beta_m^{\parallel}(z)+\beta_a^{\parallel}(z)} = \frac{P^{\parallel}(z,\lambda)C^{\parallel}K^{\parallel}}{P^{\perp}(z,\lambda)C^{\perp}K^{\perp}}, \quad (2)$$

where $\beta_m^{\perp}(z)$, $\beta_m^{\parallel}(z)$ and $\beta_a^{\perp}(z)$, $\beta_a^{\parallel}(z)$ is the molecular and particulate backscattering coefficients in the perpendicular polarization direction and parallel polarization direction, respectively; $P^{\parallel}(z,\lambda)$ and $P^{\perp}(z,\lambda)$ are the signal intensities of the perpendicular and parallel polarization channels, respectivily; $C^{\parallel}$,$K^{\parallel}$,$C^{\perp}$, and $K^{\perp}$ are the calibration and system constants for the parallel and perpendicular polarization channels, respectivily.

The extinction coefficient was calculated as

$$\alpha_a(\mathrm{z}) = \frac{\partial\left(-\frac{1}{2}\ln[T^2(z,\lambda)]\right)}{\partial z} - \alpha_m(\mathrm{z}), \quad (3)$$

where $\alpha_a(\mathrm{z})$ is the particulate extinction coefficient at height z; $T^2(z,\lambda)$ is the Two-way transmittance from height z_0 to z; $\alpha_m(\mathrm{z})$ is the molecular extinction coefficient at height z.

The lidar ratio (S) was calculated as the ratio of the particle extinction coefficient to the backscattering coefficient

$$S = \frac{\alpha_a}{\beta_a}. \quad (4)$$

https://doi.org/10.5194/egusphere-2026-6224
Preprint. Discussion started: 4 November 2026
© Author(s) 2026. CC BY 4.0 License.

Lidar ratio was used as an additional threshold in separating cloud layers from aerosols since *S* is around 15-30 sr (most typical ~19 sr) for liquid clouds, 20-50 sr for ice clouds, and 20-80 sr for various types of aerosols(Omar et al. 2009).

To evaluate cloud masks from passive imagers using ACDL, it is essential to first assess the quality of ACDL's cloud profiles. In the recently submitted paper, a one-year comparison between ACDL and CALIOP demonstrated consistent cloud patterns, with an agreement of -1.4% in total cloud fraction across all latitudes and vertical domains (Zhang et al. 2026).

2.3 Collocation and quality control

To ensure reliable comparisons, collocation between passive sensors and ACDL was performed using a temporal threshold of 10 minutes and a spatial threshold of 1 km. For each lidar profile (~5 km along-track extent), the nearest passive sensor pixel was identified and expanded along track to match the lidar footprint (±2 pixels for MODIS/MERSI-II and ±3 pixels for VIIRS, see Fig. S1). This approach ensured comparable spatial coverage between active and passive observations.

Pixel uniformity within the collocated region was used as a key quality control criterion. Analyses were conducted both including and excluding heterogeneous pixel groups to assess their impact on comparison results. Additional details of the collocation procedure and distance calculation are provided in the Appendix B.

3. Results and analysis

This section presents the key findings from the comparative analysis of cloud fraction retrievals across multiple instruments. The examination focused on the global cloud fraction distributions derived from three passive sensors, MODIS, MERSI-II, and VIIRS, and their validation against the ACDL cloud profile. The results were organized from large to small scales, encompassing global analysis and collocated monthly, day/night, and latitudinal subsets.

3.1 Global cloud fraction

A comparison of the averaged cloud fractions from Feb. and Aug. 2024 revealed consistent global patterns across the instruments (Fig. 1). The three imagers aligned well with established climatological features, such as persistent cloudiness in tropical convergence zones and surrounding Antarctica, alongside low cloud cover in subtropical subsidence regions, the Australian outback, and over the Antarctica continent. The globally averaged cloud fractions during the study periods were 66.9% for MODIS, 61.6% for MERSI-II, and 65.5% for VIIRS. As anticipated, MODIS and VIIRS exhibited greater consistency with each other (1.4%), while both detected more clouds than MERSI-II (by 5.3% and 3.9%, respectively).

However, the intercomparisons highlighted notable discrepancies, particularly in regions of high and low cloud fractions. The most pronounced differences occurred in polar regions. The MODIS-VIIRS comparison showed small positive differences over the majority of the globe, but about -10% cloud cover over the Antarctic Peninsula, with the largest difference of -38.7% at the eastern edge of the South Pole. In contrast, both MODIS-MERSI-II and VIIRS-MERSI-II comparisons indicated over 30% more clouds beyond 85° latitude, due to persistent failures in polar cloud detection within the MERSI-II algorithm.

https://doi.org/10.5194/egusphere-2026-6224
Preprint. Discussion started: 4 November 2026
© Author(s) 2026. CC BY 4.0 License.

Another major discrepancies emerged offshore along the western coasts of major continents, including North and South America, Africa, and Australia. The elevated cloud fractions off the continent may have been associated with airborne constituents, such as Sahara dust or biomass burning from central Africa, which led to misinterpretion as clouds. The large discrepancy could also be linked to the fact that the MERSI-II lacks a dedicated band for turbid water clear-sky detection, as listed in Table A1.

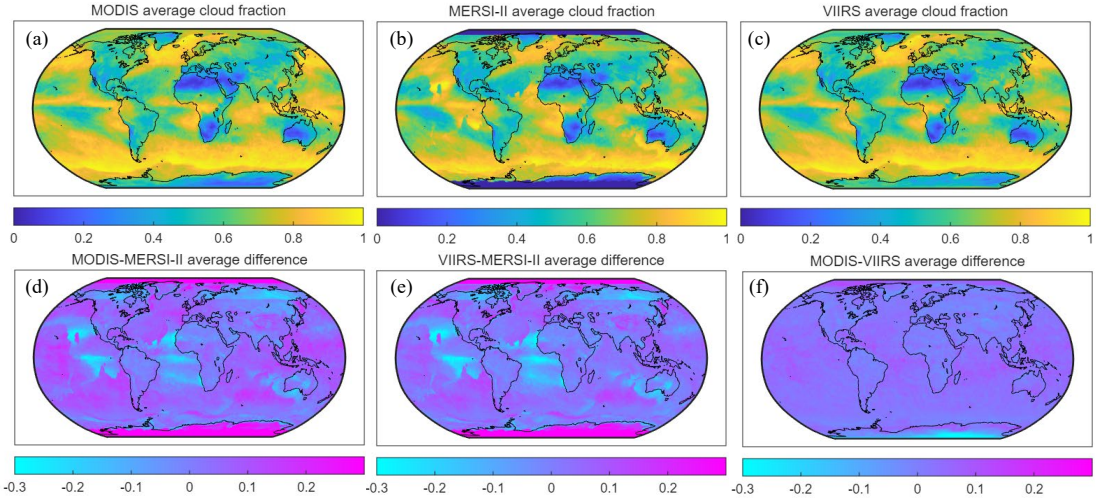


Figure 1: Global average cloud fraction (a-c) and intercomparison (d-f) among MODIS, MERSI-II, and VIIRS. Measurements from Feb. and Aug. 2024 were averaged and gridded to 1x1°. Black lines denote the coastlines.

Agreements between passive sensors themselves did not confirm accuracy, as the cloud detection of imagers was known to be less accurate under challenging conditions, such as high latitudes with low thermal contrast and high-reflectance surfaces. Figure 2 presents the averaged cloud distribution derived from ACDL profiles over the study period, aggregated to a 1° × 1° grid. The overall cloud fraction was 63.9%, which aligned with values from passive sensors and established climatological patterns. However, the ACDL-derived cloud fractions appeared higher over land and lower over oceans, particularly at high latitudes, highlighting the potential of underestimation in all passive sensor products. Direct comparisons between monthly averages would have introduced substantial sampling bias. The nadir-viewing geometry and 16-day repeat cycle of ACDL limited its sampling rate, as evidenced by the densely sampled tracks and sparsely sampled off-track grids in Fig. 2b. Therefore, in the subsequent analyses, we focused on collocated active-passive measurements within 10 min temporal and 1 km spatial proximity to enable more precise evaluations.

https://doi.org/10.5194/egusphere-2026-6224
Preprint. Discussion started: 4 November 2026
© Author(s) 2026. CC BY 4.0 License.

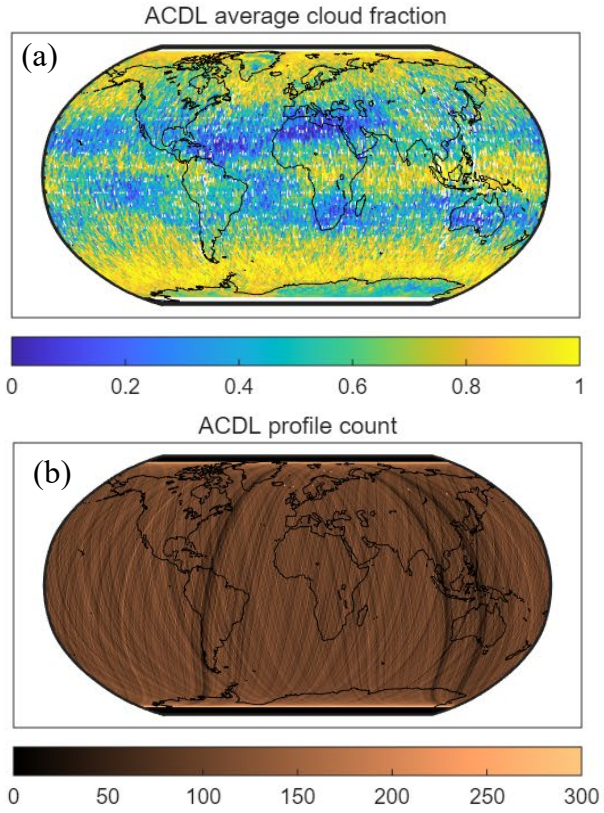


Figure 2: (a) Global average cloud fraction from ACDL and (b) profile counts from Feb. and Aug. 2024, gridded to 1x1°.

3.2 Collocated active-passive measurements

A total of 1,055,566 pairs of profiles and pixels met the spatial and temporal criteria for collocation between ACDL and MODIS; the corresponding numbers for MERSI-II and VIIRS were 803,992 and 1,063,318, respectively (Table 2). The main reason for selecting a slightly broader time range for collocation, compared to the commonly used 5-min threshold in prior studies, was to ensure a sufficient sample size. As none of the passive sensors operated on the same platform or in flying formation with ACDL, a shorter temporal threshold would have substantially reduced the sample size and increased bias toward higher latitudes. Currently, the proportion of matched pairs between 60°S and 60°N (nonpolar) accounted for 61.5% of the total for MODIS, 52.6% for MERSI-II, and 69.9% for VIIRS, with seasonal variations showing elevations in Feb. and reductions in Aug., likely attributable to minor shifts in satellite orbits.

Table 2: Total and monthly sample sizes of matched pairs for MODIS, MERSI-II, and VIIRS

Sensor	Month	Samples	Nonpolar (%)	Cloudy (%)	P.cloudy (%)	P.clear (%)	Clear (%)
MODIS	Total	1055600	61.5	66.0	5.7	6.7	21.6

https://doi.org/10.5194/egusphere-2026-6224
Preprint. Discussion started: 4 November 2026
© Author(s) 2026. CC BY 4.0 License.

	Feb	683930	65.5	65.2	5.9	7.1	21.9
	Aug	371640	54.1	67.4	5.4	6.1	21.1
MERSI-II	Total	803990	52.6	64.6	5.3	3.5	26.5
	Feb	487140	59.8	64.4	5.6	4.3	25.7
	Aug	316850	41.3	65.0	4.8	2.4	27.8
VIIRS	Total	1063318	69.9	57.7	5.6	4.9	31.8
	Feb	566983	69.8	57.2	5.6	4.5	32.7
	Aug	496335	70.0	58.2	5.5	5.3	30.9

The selection of matched pairs with an increasing fraction at high latitudes influenced the distribution of cloud mask categories. While the portion of confidently cloudy pixels (57.7-66.0%) approximated that reported in global monthly products (61.6-66.9%), these values would exceed the global average if taking the probably cloudy (P.cloudy) category into account. Although P.cloudy and probably clear (P.clear) were minor categories (<10% of the total) across all three sensors, notable discrepancies existed. The P.cloudy fractions were roughly comparable among the sensors, but P.clear fractions for MODIS and VIIRS were nearly twice those of MERSI-II, and this difference approximately matched the disparity in clear pixel fractions.

For validation against ACDL, we adopted the same method as Kotarba et al. (2020) by computing the ACDL cloudy fraction, defined as the percentage of each cloud mask category that is identified as cloudy by the lidar profile. Using ACDL as truth, an ideal cloud mask algorithm would have yield 100% ACDL cloudy identification in its cloudy category and 0% in the clear category. Analyses were conducted separately for daytime and nighttime observations, as well as for global (all latitudes) and nonpolar, since the accuracy of passive sensors was expected to vary under these conditions. In addition, an inconsistent ratio was calculated to quantify the proportion of matched pixels exhibiting heterogeneous cloud masks (i.e., mixed cloudy and clear classifications among 5 or 7 pixels). These inconsistent pixels represented a substantial fraction of the matched pairs, 16.6% on average. The values were comparable among the three sensors during daytime, but showed different degrees of increase during nighttime, with MERSI-II (26.2%) increasing more than the others (MODIS 16.7%, VIIRS 17.0%). Results for both the full dataset(using the closet pixel only for inconsistent pixels) and the consistent subset (removing inconsistent pixels) are reported in Table 3.

Table 3: Agreement between MODIS, MERSI-II, and VIIRS cloud mask product and matched ACDL profile, including statistics calculated from all data and consistent measurements only(in parentheses)

Sensor Month	Latitudes	Day/Night	Samples	Inconsistent (%)	Fraction of each category found to be cloudy by ACDL			
					Cloudy (%)	P.cloudy (%)	P.clear (%)	Clear (%)
MODIS Feb.	Global	Day	329625 (288855)	12.4	80.3 (84.6)	38.3 (37.9)	16.8 (14.5)	20.1 (18.5)

https://doi.org/10.5194/egusphere-2026-6224
Preprint. Discussion started: 4 November 2026
© Author(s) 2026. CC BY 4.0 License.

		Night	354302 (297982)	15.9	86.1 (90.6)	62.6 (60.3)	22.6 (19.3)	44.9 (45.1)
	Nonpolar	Day	233841 (200576)	14.2	76.7 (81.6)	32.1 (28.5)	14.6 (11.9)	12.2 (10.8)
		Night	214145 (177135)	17.3	80.9 (86.9)	43.2 (39.0)	15.7 (11.8)	15.3 (14.4)
MODIS Aug.	Global	Day	181554 (160161)	11.8	83.9 (87.2)	38.1 (33.9)	16.2 (13.0)	25.3 (21.9)
		Night	190085 (156773)	17.5	87.1 (91.2)	66.9 (65.2)	27.3 (25.1)	51.2 (49.7)
	Nonpolar	Day	110401 (94961)	14	74.8 (79.5)	26.6 (21.2)	12.0 (9.3)	14.8 (12.8)
		Night	90749 (74728)	17.7	80.1 (86.1)	40.3 (35.3)	17.1 (14.4)	16.7 (16.2)
MERSI-II Feb.	Global	Day	228011 (206352)	9.5	74.3 (77.5)	30.3 (27.9)	9.9 (9.0)	18.4 (17.9)
		Night	259132 (184691)	28.7	84.0 (89.1)	68.0 (60.5)	47.7 (42.3)	56.9 (53.6)
	Nonpolar	Day	149256 (133540)	10.5	71.6 (75.6)	21.5 (20.2)	7.9 (6.9)	11.1 (10.5)
		Night	142281 (107150)	24.7	80.4 (87.2)	58.7 (51.5)	42.7 (39.8)	36.5 (34.6)
MERSI-II Aug.	Global	Day	142011 (127609)	10.1	86.4 (87.8)	67.4 (66.3)	34.2 (32.7)	33.8 (31.6)
		Night	174838 (124311)	28.9	86.9 (90.8)	74.9 (71.7)	66.5 (63.8)	70.1 (68.6)
	Nonpolar	Day	67652 (61607)	8.9	79.3 (81.8)	39.0 (40.6)	13.7 (11.2)	16.2 (14.6)
		Night	63336 (48489)	23.4	85.5 (91.1)	66.4 (63.2)	61.0 (59.6)	44.2 (43.2)
VIIRS Feb.	Global	Day	270687 (236835)	12.5	83.9 (88.6)	37.8 (34.4)	20.1 (18.3)	20.9 (19.7)
		Night	296296 (243427)	17.8	85.4 (90.80)	64.1 (58.2)	42.8 (37.0)	39.4 (40.2)
	Nonpolar	Day	199846 (171450)	14.2	81.1 (86.9)	35.0 (32.1)	19.7 (18.0)	12.8 (12.0)
		Night	196034 (157098)	19.9	81.7 (88.5)	59.6 (55.4)	41.2 (35.8)	19.1 (17.8)
VIIRS Aug.	Global	Day	234096 (200487)	14.4	85.1 (89.7)	43.0 (40.0)	24.2 (21.9)	20.2 (18.0)
		Night	262239 (219826)	16.1	86.6 (91.3)	70.2 (66.1)	42.7 (37.8)	35.5 (36.0)

https://doi.org/10.5194/egusphere-2026-6224
Preprint. Discussion started: 4 November 2026
© Author(s) 2026. CC BY 4.0 License.

Nonpolar	Day	174835 (147871)	15.4	80.5 (86.5)	38.7 (37.1)	21.5 (19.3)	11.4 (10.4)
	Night	172386 (139451)	19.1	82.7 (89.3)	61.7 (58.2)	40.6 (35.9)	15.2 (13.1)

VIIRS exhibited the highest global average accuracy in cloud detection among the three sensors. The following analysis focused on consistent measurements, which exhibited slightly better performance compared to the full dataset. For the cloudy category, VIIRS achieved an average day-night ACDL cloudy confirmation rate, or true positive (TP) of 90.1%, compared to MODIS 88.4% and MERSI-II 86.3%. For the clear category, VIIRS showed the lowest false cloud detection, or false negative (FN) rate of 28.5%, compared to MODIS 33.8% and MERSI-II 42.9%. In the p.cloudy categories, VIIRS and MODIS performance were similar (49.7% vs. 49.3%), both lower than MERSI-II (56.6%), suggesting a more conservative assignment for U.S. sensors. The p.clear category followed a similar trend, with VIIRS at 28.8% positioned between MODIS (18.0%) and MERSI-II (37.0%).

Analysis of nonpolar regions showed markedly improved performance across all sensors, with substantial reductions in FN rates under clear skies. For VIIRS, the ACDL cloudy fraction in the clear category dropped from 28.5% globally to 13.3% in nonpolar areas, while MODIS decreased from 33.8% to 13.5% and MERSI-II from 42.9% to 25.7%. Accurate cloudy detection declined slightly (VIIRS: 90.1% to 87.8%, MODIS: 88.4% to 83.5%, MERSI-II: 86.3% to 83.9%), but the overall reduction in probable categories suggested enhanced reliability in non-polar areas. In other words, the evaluation highlighted the challenges posed by polar regions, which was consistent with our expectation.

Also, as expected, nighttime observations showed consistently higher error rates than daytime, primarily due to the unavailability of visible channels for clear sky detection. Even though TP got higher at night (VIIRS 91.1%, MODIS 90.9%, MERSI-II 89.9%) than in the day (VIIRS 89.2%, MODIS 85.9%, MERSI-II 82.7%), the FN rose sharply as ACDL cloudy rate showed a large increase in the remaining categories. For most subsets across sensors and seasons, the ACDL cloudy fraction in the p.cloudy category got about 1.7 times higher globally at night, while p.clear and clear categories were 2.3 times higher on average, with the largest increase reaching 4.7 times for MERSI-II (global average of Feb.). The difference was, for MODIS and VIIRS, the potential FN at night improved substantially when limited to low-mid latitudes, while the improvement was less pronounced for MERSI-II.

Monthly variations revealed that polar night conditions in Aug. generally degraded performance more than in Feb. for MERSI-II and MODIS, but less so for VIIRS, suggesting that the Antarctic polar night exerted greater influence than the Arctic. Globally, measurements in Feb. showed lower FN rates day and night for MODIS (MODIS day 18.5% vs. 21.9%, night 45.1% vs. 49.7%; MERSI-II day 17.9% vs. 31.6%, night 53.6% vs. 68.6%), but opposite for VIIRS (day 19.7% vs. 18.0%, night 40.2% vs. 36.0%). This may have stemmed from the difference between Antarctica's extensive ice-covered continent compared to the Arctic's more ocean-dominated environment. In the nonpolar region, these seasonal differences were muted, confirming that polar extremes drove most of the variance. The more balanced results from VIIRS were likely related to the more even latitude distribution of its matched samples.

https://doi.org/10.5194/egusphere-2026-6224
Preprint. Discussion started: 4 November 2026
© Author(s) 2026. CC BY 4.0 License.

To further illustrate the latitudinal distribution of matched samples and the corresponding performance of each sensor, we quantified the accuracy and inaccuracy metrics for every 10° latitude band (with latitudes > 80° aggregated into the 70-82° bin, Fig.3). Accuracy, or the hit rate, was calculated as the sum of true positives (TP) and true negatives (TN), which referred to agreed cloudy and clear classifications between the lidar profile and imager pixels. Inaccuracy, or the false-alarm rate, was calculated as the sum of false positives (FP), where the imager classified as cloudy but ACDL indicated clear, and false negatives (FN), where the opposite occurred. To incorporate the influence of probable categories in cloud mask products, two sets of metrics were calculated: one combining confident and probable categories, and the other using confident cloudy and clear results only (in parentheses).

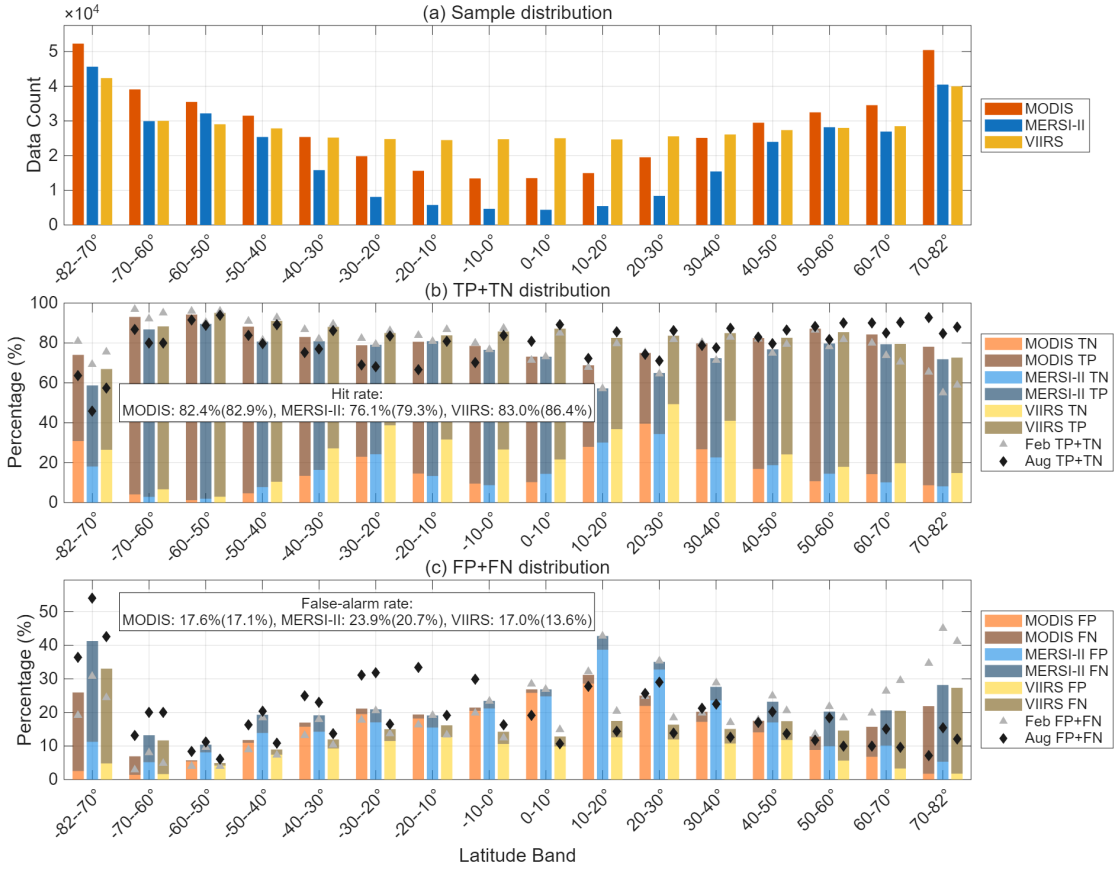


Figure 3: Latitudinal distribution of (a) collocated samples, (b) accuracy metrics, and (c) inaccuracy metrics between MODIS, MERSI-II, VIIRS, and ACDL, respectively. In panel (b), average TP and TF from Feb. and Aug. 2024 are stacked, while the monthly accuracy is indicated using symbols. Same for FP and FN in panel (c). Metrics are calculated with measurements from confident and probable categories, or confident only (in parentheses).

While all sensors showed increased sample density toward higher latitudes due to orbital convergence in polar regions, VIIRS exhibited the most balanced distribution from superior orbital alignment, as indicated by nearly 70% of collocated samples from non-polar regions, compared to 61.5% for MODIS and 52.6% for MERSI-II (Table 3). Since more samples were collected in non-polar regions, VIIRS samples showed a lower average cloud fraction than the other sensors. The overall hit

https://doi.org/10.5194/egusphere-2026-6224
Preprint. Discussion started: 4 November 2026
© Author(s) 2026. CC BY 4.0 License.

rates were 83.0% (86.4%) for VIIRS, 82.4% (82.9%) for MODIS, and 76.1% (79.3%) for MERSI-II, with VIIRS performing the best. However, VIIRS's performance may have actually been comparable to that of MODIS when accounting for its favorable sampling toward easier detection regions. The hit rate in panel 5b indicates that MODIS achieved slightly higher accuracy than VIIRS at high latitudes. Even though VIIRS's increased cloud detection during the Antarctic winter led to better agreement with ACDL in terms of monthly average cloud fraction, the cost of elevated FP diminished consistency in sample-based comparisons. In contrast, MERSI-II showed the most substantial poleward bias, with more samples clustered beyond ±60°. In addition, as the orbit of FY-3D underwent slight adjustments in 2024, there were no matched samples between 20°S-20°N in Aug.

Analysis of hit rate and false-alarm rate revealed their close association with the terrain and atmospheric circulation patterns in each latitude band. Hit rates remained high in mid-low latitudes, where TP rates increased with higher land fractions, while TN rates decreased. The north subtropical bands (10°-30°N) showed sensor-specific dips with increasing FP, potentially influenced by aerosol-laden regions of the Sahara Desert (18°-30°N), where transport dust may have confounded clear-sky detection, and complex topography over the Qinghai-Tibet Plateau (25°-40°N), where variable elevation and snow cover challenged cloud masking algorithms. In polar regions, the accuracy of all sensors declined sharply beyond ±60°, dropping to 50-70% due to increased FN rates. Seasonal variations were evident, with FN rates markedly elevated on the polar night side.

4. Discussion

In the previous section, we analyzed consistency among cloud mask products from imagers through intercomparison and validation against ACDL. Discrepancies in the results may have stemmed from various factors, including instrument design, retrieval algorithms, collocated sampling, and performance degradation over operational lifetimes. In this section, we compared the results in this work with previous studies and examined the identified influential factors (surface type, alignment conditions, aerosol loading, cirrus clouds, etc.), looking into the discrepancies while refraining from delving deep into hardware or algorithm, which fell beyond the scope of this paper.

The referenced results come from two studies comparing MODIS cloud detection results with CALIOP data. Holz et al.(2008) compared the MODIS cloud mask with CALIOP profiles using collocated samples from Aug. 2006 and Feb. 2007. Analysis of 5-min and 5-km matched samples with merging the confident and probable categories indicated global agreements of 77.0% for clear-sky conditions and 84.0% for cloudy conditions in Feb., and 75.0% for clear-sky and 85.0% for cloudy conditions in Aug. (Table 4). In this study, the comparison between MODIS and ACDL yielded slightly lower clear-sky agreements globally of 71.0% in Feb. and 64.8% in Aug, and comparable cloudy agreements at 85.9% and 87.8%, respectively. The overall consistency suggested that despite MODIS having operated continuously for 21 years (till 2024), its cloud mask product has remained stable and of high quality. The modest reduction in clear-sky accuracy may reflect differences in alignment between different platforms. Note that though both using consistent measurements, Holz et al.(2008) reported only 7% of inconsistency, much lower than the rates in this study. Compared to MODIS, VIIRS showed robustness with slight

https://doi.org/10.5194/egusphere-2026-6224
Preprint. Discussion started: 4 November 2026
© Author(s) 2026. CC BY 4.0 License.

advantages in cloudy detection during Feb., while MERSI-II showed a lower accuracy in detecting clear scenes, particularly in Aug.

Table 4: Agreement between cloud mask product and matched lidar profile compared to results in Holz et al.(2008), including statistics calculated from all data and confident data only (in parentheses).

Agreement between cloud mask product and the lidar profile				
	Feb. clear	Feb. cloudy	Aug. clear	Aug. cloudy
Holz et al. based on Aug.2006 and Feb.2007				
MODIS vs. CALIOP				
Global 5km	77.0	84.0	75.0	85.0
Nonpolar ocean	79.0	86.0	83.0	86.0
Nonpolar land	74.0	81.0	86.0	78.0
This work based on Feb. 2024 and Aug.2024				
MODIS vs. ACDL				
Global 5km	71.0 (67.9)	85.9 (87.6)	64.8 (61.1)	87.8 (89.0)
Nonpolar ocean	92.1 (93.3)	82.7 (83.5)	91.9 (92.9)	80.6 (81.4)
Nonpolar land	82.8 (83.8)	80.6 (85.7)	82.4 (83.2)	81.4 (87.0)
MERSI-II vs. ACDL				
Global 5km	59.1 (56.1)	80.1 (81.9)	42.2 (41.3)	88.3 (89.0)
Nonpolar ocean	75.6 (73.9)	79.1 (79.8)	67.4 (67.4)	85.1 (85.5)
Nonpolar land	73.5 (72.3)	74.4 (80.1)	69.2 (69.5)	81.9 (84.9)
VIIRS vs. ACDL				
Global 5km	69.7 (69.5)	87.7 (89.7)	71.4 (71.9)	88.9 (90.5)
Nonpolar ocean	88.1 (90.4)	86.2 (87.3)	88.1 (90.6)	86.6 (87.8)
Nonpolar land	77.4 (78.2)	83.8 (88.5)	82.4 (85.2)	83.7 (87.9)

Holz et al.(2008) further stratified the results by surface type, revealing that agreements over ocean surfaces were generally higher than over land in nonpolar regions, with most pronounced disparity in cloudy detection in Aug. (86.0% ocean vs. 78.0% land). This pattern may be attributed to greater thermal and spectral contrasts over water, facilitating more reliable cloud discrimination. The present study aligned with this trend; for MODIS vs. ACDL, the agreements over the ocean were 86.6% on average, higher than 82.1% over land in nonpolar regions. Similar consistencies hold for MERSI-II (ocean average 78.1% vs. land 75.2%) and VIIRS (ocean 87.3% vs. land 81.7%).

Similarly, Kotarba et al. (2020) compared the MODIS cloud mask with CALIOP profiles from Jan. and Jul. 2015 and matched with 5-min/1-km alignment. Their analysis reported the fraction of each cloud mask category classified as cloudy by CALIOP as follows: 94.7% for confident cloudy, 66.6% for probably cloudy, 27.7% for probably clear, and 21.5% for

https://doi.org/10.5194/egusphere-2026-6224
Preprint. Discussion started: 4 November 2026
© Author(s) 2026. CC BY 4.0 License.

confident clear (Table 5). The global consistency for the 1-km match tends to be higher than the 5-km match, especially for clear scenes (85% vs. 77% in Holz et al.(2008)). Consequently, the results from the present study, comparing MODIS and ACDL at the global 5-km scale, showed acceptably lower fractions for confident cloudy at 84.4% (88.4% for consistent data only), and higher fractions for confident clear at 35.4% (33.8%). The day-night pattern aligned, with nighttime FP rates substantially higher in the clear categories in all comparisons. VIIRS demonstrated slightly higher confidence cloudy fractions of 85.2% (90.1%) and lower confidence clear fractions of 29.0% (28.5%), indicating fewer missed clouds, while MERSI-II showed opposite trends, pointing to greater tendencies for undetected clouds, especially at night.

Table 5: Fraction of each cloud mask category found to be cloudy by lidar profile compared to results in Kotarba et al.(2020), including statistics calculated from all data and consistent data only (in parentheses).

The fraction of each category found to be cloudy by lidar profile.				
	Cloudy (%)	P.cloudy (%)	P.clear (%)	Clear (%)
Kotarba et al. based on Jan. and Jul. 2015				
MODIS vs. CALIOP				
Global 1km	94.7	66.6	27.7	21.5
Day only	94.7	58.4	28.4	12.7
Night only	94.7	70.7	27.1	29.5
This work based on Feb. and Aug. 2024				
MODIS vs. ACDL				
Global 5km	84.4 (88.4)	51.5 (49.3)	20.7(18.0)	35.4(33.8)
Day only	82.1 (85.9)	38.2 (35.9)	16.5(13.7)	22.7(20.2)
Night only	86.6 (90.9)	64.7 (62.7)	25.0(22.2)	48.0(47.4)
MERS-II vs. ACDL				
Global 5km	82.9 (86.3)	60.1 (56.6)	39.6 (36.9)	44.8 (42.9)
Day only	80.3 (82.7)	48.8 (47.1)	22.1 (20.9)	26.1 (24.7)
Night only	85.5 (90.0)	71.5 (66.1)	57.1 (53.1)	63.5 (61.1)
VIIRS vs. ACDL				
Global 5km	85.3 (90.1)	53.8 (49.7)	32.5 (28.8)	29.0 (28.5)
Day only	84.5(89.2)	40.4 (37.2)	22.29 (20.1)	20.5 (18.8)
Night only	86.0 (91.1)	67.1 (62.1)	42.7 (37.4)	37.5 (38.1)

Given the significant influence of surface type on cloud mask performance, we examined the distributions of surface types and ice/snow cover in the matched samples across MODIS, MERSI-II, and VIIRS (Fig. 4). The results revealed reasonable and highly consistent distributions for water and non-water surfaces, and ice/snow cover, with variations aligning with seasonal patterns and latitudinal sample distributions. However, the sub-classification between land and desert surfaces

https://doi.org/10.5194/egusphere-2026-6224
Preprint. Discussion started: 4 November 2026
© Author(s) 2026. CC BY 4.0 License.

appeared distinct for MERSI-II, particularly in polar regions, where it classified approximately 30% more land surfaces than the other two sensors, indicating significant differences in its definition or classification between land and desert surface types.

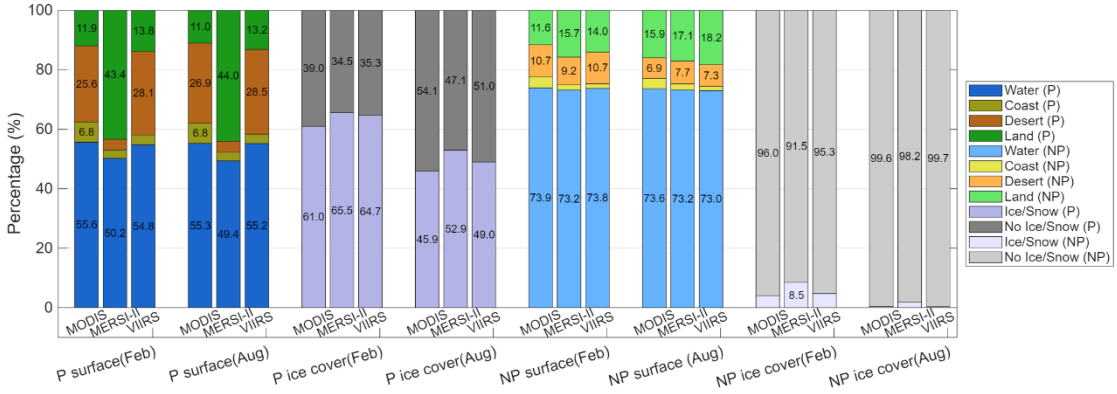


Figure 4: Percentage distribution of surface types and ice/snow cover in polar and non-polar regions based on matched samples of cloud detection between MODIS, MERSI-II, VIIRS, and ACDL from Feb. and Aug. 2024. Bars are grouped by sensor, with dark colors indicating polar (P) and light colors indicating non-polar (NP) regions.

The percentage contributions of deserts and ice/snow (highly reflective surfaces), along with other environmental and observational factors to FP, FN, and inconsistencies among imager pixels are illustrated in Fig.5. As expected, ice/snow-covered pixels contributed substantially to FN samples, approximately twice those observed in FP for all sensors, especially for MODIS. Desert surfaces exhibited comparable contributions in FP and FN (33.9% versus 33.0% for MODIS, 37.7% versus 31.0% for MERSI-II, and 39.2% versus 31.0% for VIIRS), indicating a balanced challenge for the retrieval algorithm. Dawn/dusk periods (solar zenith angles between 80°-90°), characterized by poor and rapidly changing illumination conditions, showed slightly higher contributions to FN than to FP. Sunglint showed a negligible impact, except for VIIRS (14.1% and 9.1%). High aerosol loading (ACDL-retrieved AOD >1 at 532 nm) accounted for 12.7-26.4% of FP across the sensors, which was minimal in FN, aligning with expectations. Thin cirrus clouds (ACDL-retrieved cloud top height >6 km and geometric thickness <1 km), another known challenge in passive cloud retrievals, contributed 17-21% to FN, also consistent with anticipations. Larger time differences (>5 min) would theoretically impact matching accuracy, yet their contributions remained at or below approximately half of the samples, with no significant difference between FP and FN. This suggested that the 10-min threshold did not introduce excessive discrepancies relative to 5-min threshold. Note that different factors can overlap, and there were still portions of the samples that did not align with any of the analyzed factors. The possibility of additional unidentified influences remains.

https://doi.org/10.5194/egusphere-2026-6224
Preprint. Discussion started: 4 November 2026
© Author(s) 2026. CC BY 4.0 License.

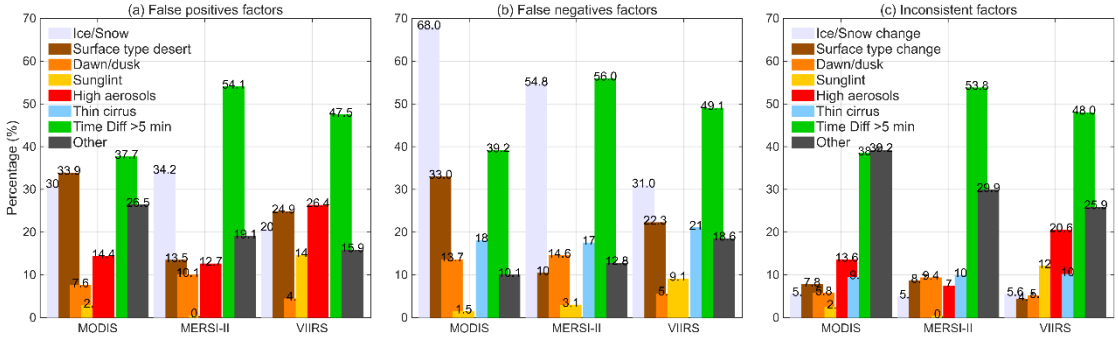


Figure 5:Percentage contributions of environmental and observational factors to false positives (a), false negatives (b), and inconsistencies (c) based on matched samples of cloud detection between MODIS, MERSI-II, VIIRS, and ACDL from Feb. and Aug. 2024.

For inconsistent pixels, the analysis emphasized the causes of discrepancies in cloud mask within proximate spatiotemporal domains and focused on potential changes therein. Variations in ice/snow coverage and surface types indicate difficult geographics, while dawn/dusk and sunglint reflect fast-changing illumination conditions, and aerosols and cirrus clouds represent complex atmospheric backgrounds. However, apart from high aerosol loadings contributing about one-fifth (25.9%) of heterogeneous results for VIIRS, these factors exhibited generally low contributions across sensors. This implies that inconsistencies were more likely attributable to rapid variations in the cloud layers, such as edged or fractus characteristics. Improving the spatio-temporal resolution of passive remote sensors and their alignment with lidar observations might be more effective strategies for mitigating such inconsistencies.

5. Conclusion

In this study, we evaluated the performance of cloud mask products from three passive satellite imagers, Aqua/MODIS, FY-3D/MERSI-II, and NOAA-21/VIIRS, by validating them against cloud profiles from the space-borne lidar ACDL as a reference truth. Monthly cloud fractions and collocated samples from granule-based measurements are analyzed from Feb. and Aug. 2024, encompassing seasonal, day/night, and latitudinal subsets to assess agreement and discrepancies. The global average hit rates reached 86.4% for VIIRS, 82.9% for MODIS, and 79.3% for MERSI-II based on pixels classified as confident cloudy or clear, with patterns aligning closely with prior validations between MODIS and CALIOP. The high accuracy in general confirms the enduring stability of the three sensors and their algorithms, with certain variations under specific conditions.

VIIRS demonstrated superior performance relative to the others, evidenced by the most balanced hit rate across different subsets. The fractions of VIIRS cloud mask categories classified as cloudy by ACDL were 90.1% for confident cloudy, 49.7% for probably cloudy, 28.8% for probably clear, and 28.5% for confident clear on average, compared to 88.4%, 49.3%, 18.0%, and 33.8% for MODIS, and 86.3%, 56.6%, 36.9%, and 42.9% for MERSI-II, respectively. Detailed analyses of latitude bands showed increases in FP at low latitudes due to Sahara dust transport and complex topography over the Qinghai-Tibet Plateau.

https://doi.org/10.5194/egusphere-2026-6224
Preprint. Discussion started: 4 November 2026
© Author(s) 2026. CC BY 4.0 License.

Day/night subsets indicated that VIIRS maintained the lowest escalation at night, with FN increasing by 1.9 times, compared to 2.3 times for MODIS and 2.5 times for MERSI-II. Assessments of monthly fraction revealed that VIIRS has the right tendency of increasing overall cloud detection in Antarctic winter, but sample-based analysis showed potential improvement in accuracy being overridden by increasing FP.

The study also demonstrates ACDL's value as a reliable benchmark for the validation of cloud products, especially in regions with high false-alarm rates for all passive sensors. Several key factors were identified from possible reasons complicating cloud retrieval algorithms or matching precision. Ice/snow cover and thin cirrus clouds contributed more to FN, high aerosol loading contributed to FP, and desert surfaces and dawn/dusk illumination contributed to both sides.

The assessment revealed that alignment between imagers and lidar impacts evaluation outcomes. VIIRS benefited from optimal collocation with ACDL, including orbit design and finer spatial resolution, which led to more even sample distribution (69.9% non-polar samples vs. 61.5% for MODIS vs. 52.6% for MERSI-II), which implies that the actual accuracy gap among sensors is smaller than apparent. Given the inheritance between MODIS and VIIRS, their close match in precision and patterns is reasonable. In contrast, MERSI-II underperformed particularly in clear-sky detection over polar regions and at night; further improvements in handling low thermal contrasts over ice/snow-covered surfaces are necessary.

The performance and consistency validated in this work among passive sensors are vital not only for validating the accuracy of individual cloud masks but also for their combined usage in merging datasets and models for long-term studies. Considering operational stages, VIIRS onboard NOAA-21 is the latest payload used in the study, while Aqua/MODIS has maintained robust performance after over two decades of operation, which is highly encouraging. FY-3D, on the other hand, is designed for a much shorter 7-year lifespan and is now nearing its operational end. The results of this study provide suggestions for the new afternoon-orbit satellite of the FY-3 series, FY-3H launched in Dec. 2025.

Appendix A: Passive instrument description

By design, MODIS is a whiskbroom scanner with 36 spectral channels spanning the visible (VIS), near-infrared (NIR), shortwave infrared (SWIR), and thermal infrared (TIR) regions(0.4-14.4 μm). MERSI-II is a pushbroom scanner with 25 spectral channels covering VIS to TIR (0.47-12.0 μm). VIIRS is a whiskbroom scanner with 22 spectral bands covering VIS to TIR (0.412-12 μm). The success of MODIS has profoundly inspired the development of the FY-3 series, both for instrument and product design. VIIRS serves as the official successor to MODIS, integrating its most critical features to maintain continuity in cloud observation. The interconnections among passive sensors, especially the similarity in the product design, greatly facilitated the cross-sensor comparisons in this study.

In its C6.1 updates, MODIS cloud detection algorithm employs up to 19 multispectral thresholds and consistency tests, including visible reflectance thresholds, infrared brightness temperature differences (e.g., 11-12 μm split-window), and spatial variability checks(Table 2). The principle relies on exploiting spectral contrasts between clouds and underlying surfaces, such as high reflectance in VIS/NIR for clouds over dark oceans or land, and TIR emission differences for cloud top detection, with

https://doi.org/10.5194/egusphere-2026-6224
Preprint. Discussion started: 4 November 2026
© Author(s) 2026. CC BY 4.0 License.

additional tests for cirrus and heavy aerosols. Based on these, a clear-sky confidence level (clear, probably clear, probably cloudy, cloudy) is assigned to each pixel, and a cloud mask product (MYD35_L2) is generated at 1 km and 5 min intervals [23]. Additionally, the MODIS cloud mask also encodes surface type (water, coastal, desert, and land), snow/ice presence, day/night conditions, and sun glint in its bit field. These flags were utilized in our analysis of cross-sensor comparison to categorize and refine pixel selection and account for environmental variability. Geolocation data for MYD35, including 1-km resolution latitude and longitude, were obtained from the corresponding MYD03 product.

Monthly cloud fraction of 1x1° was extracted from the L3 monthly cloud properties product(CLDPROP_M3_MODIS_Aqua), which was derived by aggregating the daily Aqua/MODIS D3 Cloud Properties product. Mentioned products are available at the Level-1 and Atmosphere Archive & Distribution System Distributed Active Archive Center (LAADS DAAC) online.

VIIRS has fewer bands compared to MODIS, missing water vapor absorption channels at 6.7 and 7.3 μm, and the CO2 absorption band at 13.3 μm can make a difference in the detection of clear skies in polar night conditions. A continuity MODIS-VIIRS cloud mask (MVCM) was designed to facilitate the transition from MODIS on the Aqua and Terra platforms to the series of VIIRS onboard Soumi NPP and other platforms, utilizing only those channels that are common to both instruments. The VIIRS L2 cloud mask product (CLDMSK_L2_VIIRS_NOAA21) is also provided at LAADS DAAC with the same structure as MODIS. L3 monthly cloud properties for NOAA-21/VIIRS were not available yet, so we aggregated 1x1° monthly cloud fraction from the L2 product. Geolocation data for VIIRS has been included in the L2 package; therefore, no longer needed to download separately.

Compared to MODIS and VIIRS, MERSI-II onboard FY-3D has a slightly different channel design, but the cloud masking algorithm follows the same ideology. A combination of fixed/dynamic thresholds on VIS reflectance, NIR/SWIR ratios, and TIR brightness temperature differences is applied to measured radiances, and ancillary flags are also recorded in the product. L2 cloud mask product MERSI-II Cloud Mask (Granule) and L3 0.05x0.05° monthly cloud fraction product Cloud Amount (Monthly) are available at FENGYUN Satellite Data Service online.

Table A1:MODIS, VIIRS, and MERSI-II spectral bands used in their cloud mask algorithms

Spectral Bands Used in the MODIS, VIIRS, and MERSI-II Cloud Mask				
Wavelengths (μm)	MODIS Band	VIIRS Band	MERSI-II Band (with adjustment)	Primary Use
0.412	8	M1	8	daytime desert cloud detection
0.443	9	M2	9	sun glint clear sky detection
0.555	4	M4	11 (0.550)	snow/ice detection
0.645	1	M5	3(0.650)	land surface cloud detection
0.859	2	M7	4(0.865)	water surface cloud detection
1.24	5	M8	not use	turbid water clear sky detection

https://doi.org/10.5194/egusphere-2026-6224
Preprint. Discussion started: 4 November 2026
© Author(s) 2026. CC BY 4.0 License.

1.375	26	M9	1.38(19)	transmissive cirrus cloud detection
1.64	6	M10	6	snow/ice detection, water surface cloud detection
2.13	7	M11	7	snow/ice detection, water surface cloud detection
3.75	20	M12	20(3.8)	land and water surface cloud detection
3.96	21	not used	not used	land and water surface cloud detection
8.55	29	M14	23	water surface ice cloud detection
11.03	31	M15	24(10.8)	night land and water surface cloud detection
12.02	32	M16	25(12.0)	transmissive cirrus cloud detection

Appendix B: Collocation method

In this study, we used the official L2 cloud mask and the monthly L3 cloud fraction in the cloud properties package from each passive sensor. As noted before, MODIS, MERSI-II, and VIIRS have inherent similarity in their instrument configuration, which continued in the retrieval algorithm and product design.

ACDL profiles contain the attenuated backscatter coefficients in the parallel channel, perpendicular channel, and molecular channel. In the pre-processing, 2 vertical bins in each profile and 15 profiles along the track were averaged to improve SNR, resulting in vertical resolution of 48 m and along-track resolution of 5 km. Atmospheric profiles obtained from the ERA5 model were used to calculate the atmospheric molecular number density, deriving the backscattering and extinction profiles of atmospheric molecules, serving as inputs for the layer identification algorithm. Backscatter coefficient ratio (R_a) was then calculated as the relative magnitude between particle and molecular signals.

The active and passive sensors used in this study were launched onboard separate platforms, which required time and spatial thresholds to match high-quality collocated pixels. A temporal threshold of 10 min and a spatial threshold of 1 km were employed as the collocation criteria to ensure proximity. For a passive sensor, the time of each granule is measured for every pixel, while for ACDL, a timestamp is recorded for each profile. Distances between collocation points were calculated using the Haversine formula,

$$d = 2r \cdot \arcsin\sqrt{\left(\sin^2\left(\frac{\phi 1-\phi 2}{2}\right) + \cos\phi 1 \cdot \cos\phi 2 \cdot \sin^2\left(\frac{\lambda 1-\lambda 2}{2}\right)\right)}, \quad \text{(B1)}$$

where d is the spatial distance, $\lambda 1$ and $\lambda 2$ are the longitude, $\phi 1$, and $\phi 2$ are the latitude of the lidar footprint and image pixels, respectively, and r represents the Earth's radius.

Each lidar cloud profile is derived from 15 consecutive measurements spaced 333 m apart along the track, spanning approximately 5 km. Spatial collocation was achieved by first identifying the closest 1×1 km MODIS or MERSI-II pixel to each lidar footprint, followed by incorporating ±2 adjacent pixels along the track direction to form a 1×5 km coverage area

https://doi.org/10.5194/egusphere-2026-6224
Preprint. Discussion started: 4 November 2026
© Author(s) 2026. CC BY 4.0 License.

(Fig. B1). For VIIRS, with its nominal pixel resolution of 0.75×0.75 km, the process included ±3 pixels along the track relative to the central matched pixel, resulting in a total of 7 pixels to approximate the same 5 km extent. The uniformity among these adjacent pixels served as a key quality control criterion. Accordingly, our analysis was performed both with and without collocation pairs exhibiting heterogeneous cloud masks, while also investigating potential factors contributing to observed discrepancies.

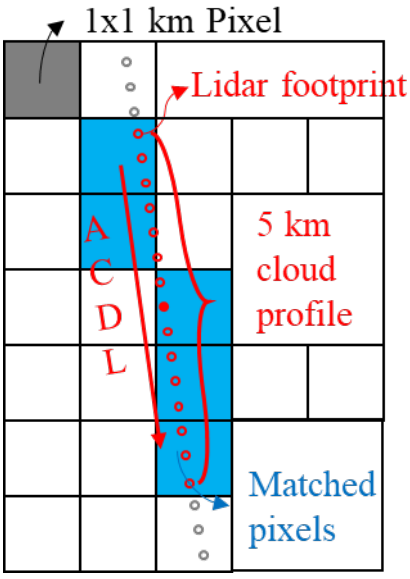


Figure B1:Demonstration of collocation between image pixels and lidar cloud profile.

Declaration of competing interest

The authors report no conflict of interest.

Data availability statement

The datasets analyzed in this study are publicly available from the respective satellite data archives. MODIS and VIIRS cloud products were obtained from the NASA Level-1 and Atmosphere Archive & Distribution System Distributed Active Archive Center (LAADS DAAC) at https://ladsweb.modaps.eosdis.nasa.gov/search/.

FY-3D/MERSI-II products were downloaded from the National Satellite Meteorological Center (NSMC) data portal at http://data.nsmc.org.cn/DataPortal/en/code/index.html?code=Atmosphere.

ACDL products used for cloud profile retrievals were released in L2C cloud and aerosols product, which could be downloaded from scientific data portal at http://210.45.127.184:8081/.

https://doi.org/10.5194/egusphere-2026-6224
Preprint. Discussion started: 4 November 2026
© Author(s) 2026. CC BY 4.0 License.

Financial support

This work was supported by the National Key R&D Program of China (2023YFB3906000).

Author contributions

Sijie Chen: Conceptualization, Methodology, Formal analysis, Investigation, Writing - original draft, Visualization, Validation; Bo Li: Conceptualization, Supervision, Writing - review & editing; Xi Wang: Data curation, Resources, Validation; Zhaojun Zheng: Data curation, Resources, Software; Lin Chen: Conceptualization, Funding acquisition, Supervision, Project administration; Jian Liu: Conceptualization, Supervision, Writing - review & editing.
All authors have read and approved the final version of the manuscript.

References

Ackerman, S. A., R. E. Holz, R. Frey, E. W. Eloranta, B. C. Maddux, and M. McGill. 2008. "Cloud Detection with Modis. Part Ii: Validation." *Journal of Atmospheric and Oceanic Technology* 25, no. 7 (Jul): 1073-1086. https://dx.doi.org/10.1175/2007jtecha1053.1.

Ackerman, S. A., K. I. Strabala, W. P. Menzel, R. A. Frey, C. C. Moeller, and L. E. Gumley. 1998. "Discriminating Clear Sky from Clouds with Modis." *Journal of Geophysical Research-Atmospheres* 103, no. D24 (Dec 27): 32141-32157. https://dx.doi.org/10.1029/1998jd200032.

Baum, BA, WP Menzel, RA Frey, DC Tobin, RE Holz, SA Ackerman, AK Heidinger, and P Yang. 2012. "Modis Cloud-Top Property Refinements for Collection 6." *JOURNAL OF APPLIED METEOROLOGY AND CLIMATOLOGY* 51, no. 6 (2012-06-01): 1145-1163. https://dx.doi.org/10.1175/JAMC-D-11-0203.1.

Chen, Sijie, Bo Li, Zhang Lu, Lu Zhang, and Lin Chen. 2025. *The Feasibility and Potential of near-Synchronous Observations between Dq-1/Acdl and Fy-3/Mersi*. Vol. 13511. *Proc.SPIE*. https://doi.org/10.1117/12.3057212

Chen, Weibiao, Jiqiao Liu, Xia Hou, Huaguo Zang, Xiuhua Ma, Yuan Wan, and Xiaopeng Zhu. 2023. *Lidar Technology for Atmosphere Environment Monitoring Satellite*. Vol. 40. Aerospace Shanghai (Chinese & English). https://doi.org/10.19328/j.cnki.2096-8655.2023.03.002

Dai, G., S. Wu, W. Long, J. Liu, Y. Xie, K. Sun, F. Meng, X. Song, Z. Huang, and W. Chen. 2024. "Aerosol and Cloud Data Processing and Optical Property Retrieval Algorithms for the Spaceborne Acdl/Dq-1." *Atmos. Meas. Tech.* 17, no. 7: 1879-1890. https://dx.doi.org/10.5194/amt-17-1879-2024.

Frey, RA, SA Ackerman, RE Holz, S Dutcher, and Z Griffith. 2020. "The Continuity Modis-Viirs Cloud Mask." *REMOTE SENSING* 12, no. 20 (2020-10-01). https://dx.doi.org/10.3390/rs12203334.

Holz, R. E., S. A. Ackerman, F. W. Nagle, R. Frey, S. Dutcher, R. E. Kuehn, M. A. Vaughan, and B. Baum. 2008. "Global Moderate Resolution Imaging Spectroradiometer (Modis) Cloud Detection and Height Evaluation Using Caliop." *Journal of Geophysical Research-Atmospheres* 113 (Dec 19). https://dx.doi.org/10.1029/2008jd009837.

Ke, Ju, Yingshan Sun, Changzhe Dong, Xingying Zhang, Zijun Wang, Liqing Lyu, Wei Zhu, Albert Ansmann, Lin Su, Lingbing Bu, Da Xiao, Shuaibo Wang, Sijie Chen, Jiqiao Liu, Weibiao Chen, and Dong Liu. 2022. "Development of China's First Space-Borne Aerosol-Cloud High-Spectral-Resolution Lidar: Retrieval Algorithm and Airborne Demonstration." *Photonix* 3, no. 1 (Jul 26). https://dx.doi.org/10.1186/s43074-022-00063-3.

https://doi.org/10.5194/egusphere-2026-6224
Preprint. Discussion started: 4 November 2026
© Author(s) 2026. CC BY 4.0 License.

Kim, SW, ES Chung, SC Yoon, BJ Sohn, and N Sugimoto. 2011. "Intercomparisons of Cloud-Top and Cloud-Base Heights from Ground-Based Lidar, Cloudsat and Calipso Measurements." *INTERNATIONAL JOURNAL OF REMOTE SENSING* 32, no. 4 (2011-01-01): 1179-1197. https://dx.doi.org/10.1080/01431160903527439.

Kopp, TJ, W Thomas, AK Heidinger, D Botambekov, RA Frey, KD Hutchison, BD Iisager, K Brueske, and B Reed. 2014. "The Viirs Cloud Mask: Progress in the First Year of S-Npp toward a Common Cloud Detection Scheme." *JOURNAL OF GEOPHYSICAL RESEARCH-ATMOSPHERES* 119, no. 5 (2014-03-16): 2441-2456. https://dx.doi.org/10.1002/2013JD020458.

Kotarba, AZ. 2020. "Calibration of Global Modis Cloud Amount Using Caliop Cloud Profiles." *ATMOSPHERIC MEASUREMENT TECHNIQUES* 13, no. 9 (2020-09-25): 4995-5012. https://dx.doi.org/10.5194/amt-13-4995-2020.

Liu, D, YY Yang, ZT Cheng, HL Huang, B Zhang, T Ling, and YB Shen. 2013. "Retrieval and Analysis of a Polarized High-Spectral-Resolution Lidar for Profiling Aerosol Optical Properties." *OPTICS EXPRESS* 21 (2013-06-03): 13084-13093. https://dx.doi.org/10.1364/OE.21.013084.

Liu, Q., Z. Huang, J. Liu, W. Chen, Q. Dong, S. Wu, G. Dai, M. Li, W. Li, Z. Li, X. Song, and Y. Xie. 2024. "Validation of Initial Observation from the First Spaceborne High-Spectral-Resolution Lidar with a Ground-Based Lidar Network." *Atmos. Meas. Tech.* 17, no. 5: 1403-1417. https://dx.doi.org/10.5194/amt-17-1403-2024.

Meyer, K, S Platnick, R Holz, S Dutcher, G Quinn, and F Nagle. 2020. "Derivation of Shortwave Radiometric Adjustments for Snpp and Noaa-20 Viirs for the Nasa Modis-Viirs Continuity Cloud Products." *REMOTE SENSING* 12, no. 24 (2020-12-01). https://dx.doi.org/10.3390/rs12244096.

Omar, AH, DM Winker, C Kittaka, MA Vaughan, ZY Liu, YX Hu, CR Trepte, RR Rogers, RA Ferrare, KP Lee, RE Kuehn, and CA Hostetler. 2009. "The Calipso Automated Aerosol Classification and Lidar Ratio Selection Algorithm." *JOURNAL OF ATMOSPHERIC AND OCEANIC TECHNOLOGY* 26, no. 10 (2009-10-01): 1994-2014. https://dx.doi.org/10.1175/2009JTECHA1231.1.

Sedano, F, P Kempeneers, P Strobl, J Kucera, P Vogt, L Seebach, and J San-Miguel-Ayanz. 2011. "A Cloud Mask Methodology for High Resolution Remote Sensing Data Combining Information from High and Medium Resolution Optical Sensors." *ISPRS JOURNAL OF PHOTOGRAMMETRY AND REMOTE SENSING* 66, no. 5 (2011-09-01): 588-596. https://dx.doi.org/10.1016/j.isprsjprs.2011.03.005.

Thorsen, TJ, Q Fu, and J Comstock. 2011. "Comparison of the Calipso Satellite and Ground-Based Observations of Cirrus Clouds at the Arm Twp Sites." *JOURNAL OF GEOPHYSICAL RESEARCH-ATMOSPHERES* 116 (2011-11-10). https://dx.doi.org/10.1029/2011JD015970.

Winker, DM, MA Vaughan, A Omar, YX Hu, KA Powell, ZY Liu, WH Hunt, and SA Young. 2009. "Overview of the Calipso Mission and Caliop Data Processing Algorithms." *JOURNAL OF ATMOSPHERIC AND OCEANIC TECHNOLOGY* 26 (2009-11-01): 2310-2323. https://dx.doi.org/10.1175/2009JTECHA1281.1.

Wu, W, JC Luo, XD Hu, HP Yang, and YP Yang. 2018. "A Thin-Cloud Mask Method for Remote Sensing Images Based on Sparse Dark Pixel Region Detection." *REMOTE SENSING* 10, no. 4 (2018-04-01). https://dx.doi.org/10.3390/rs10040617.

Xiong, XX, A Angal, JQ Sun, N Lei, K Twedt, HD Chen, and K Chiang. 2023. *An Overview of Noaa-21 Viirs Early on-Orbit Calibration and Performance*. Vol. 12729. *SENSORS, SYSTEMS, AND NEXT-GENERATION SATELLITES XXVII*. https://doi.org/10.1117/12.2680636

https://doi.org/10.5194/egusphere-2026-6224
Preprint. Discussion started: 4 November 2026
© Author(s) 2026. CC BY 4.0 License.

Zhang, Kai, Sijie Chen, Haodong Yu, Shiping Guo, and Tingkui Mu. 2026. "Acdl/Dq-1 Measurements of Global Cloud Heights and Geometric Thickness: Results and Intercomparison with Caliop Products." *International Journal of Remote Sensing* 47, no. 14 (2026/07/18): 6113-6131. https://dx.doi.org/10.1080/01431161.2026.2680266.